Raman scattering probe of ion-implanted and pulse laser annealed GaAs

Prabhat Verma,[a] K. P. Jain, and S. C. Abbi
Department of Physics, Indian Institute of Technology, Delhi, New Delhi 110 016, India

(Received 30 May 1995; accepted for publication 18 December 1995)

We report Raman scattering studies of phosphorus-ion-implanted and subsequently pulse laser annealed (PLA) GaAs. The threshold value of implantation fluence for the disappearance of one-phonon modes in the Raman spectrum of ion-implanted GaAs sample is found to be greater than that for the two-phonon modes by an order of magnitude. The phonon correlation length decreases with increasing disorder. The lattice reconstruction process during PLA creates microcrystallites for incomplete annealing, whose sizes can be given by the phonon correlation lengths, and are found to increase with the annealing power density. The intensity ratio of the Raman spectra corresponding to the allowed longitudinal-optical (LO)-phonon mode to the forbidden transverse-optical (TO)-phonon mode, $I_{\mathrm{LO}}/I_{\mathrm{TO}}$, is used as a quantitative measure of crystallinity in the implantation and PLA processes. The threshold annealing power density is estimated to be 20 MW/cm^2 for 70 keV phosphorus-ion-implanted GaAs at a fluence of 5×10^{15} ions/cm^2. The localized vibrational mode of phosphorus is observed in PLA samples for fluences above 1×10^{15} ions/cm^2. © *1996 American Institute of Physics.* [S0021-8979(96)01807-X]

I. INTRODUCTION

Ion implantation[1–5] is a method of obtaining the desired impurity profile in a controlled way, and pulse laser annealing (PLA) of ion-implanted samples gives charge carrier activation and better lattice reconstruction compared to conventional annealing methods. Ion implantation followed by PLA has therefore become an ideal scientific tool for the development of fast electronics device technology. Consequently, the microscopic understanding of ion implantation and PLA is of great technological importance, especially for such systems as GaAs, which is finding increasing applications in semiconductor devices. Raman spectroscopy is a powerful nondestructive technique for probing the atomic scale structure in implanted and PLA layer of a semiconductor. A quantitative distinction between a crystalline lattice and a lattice with some degree of disorder can be made by Raman scattering.[6,7]

The ⟨100⟩ face of a GaAs sample was implanted with 70 keV phosphorus ions (P-ions) at various implantation fluences. The sample with implantation fluence of 5×10^{15} ions/cm^2 was annealed using a *Q*-switched Nd:YAG laser with various annealing power densities. The degree of disorder and the threshold value of implantation fluence for complete amorphization in the implantation process were estimated using Raman scattering experiments. Raman scattering was also used to estimate the degree of recrystallization and the threshold value of annealing power density for complete recrystallization. Some investigations[4,7,8] on this problem are reported in the literature, but little[4] or no attention has been paid to two-phonon structures, probably because they are very weak. The discussion in the literature on the degree of disorder in such samples is generally very qualitative. Our spectra are significantly cleaner and more complete (observed down to 20 cm^{-1} before appreciable competition appears from the Rayleigh scattering) than most of earlier data.

The aim of this article is to make a comparative study of various intermediate states of GaAs from crystalline to amorphous during P-ion implantation and from amorphous to crystalline during the PLA as monitored by room temperature Raman scattering experiments. In this article, the ratio of Raman intensities of the allowed longitudinal-optical (LO)-phonon mode to the forbidden transverse-optical (TO)-phonon mode ($I_{\mathrm{LO}}/I_{\mathrm{TO}}$), is used as a quantitative measure of the relative degree of disorder produced during the implantation process and to compare the relative degree of recrystallization in the reverse PLA process. The threshold fluence during the ion implantation process has been estimated for the complete disappearance of one-phonon mode and the two-phonon modes, and these are found to be different from each other. The size of microcrystallites produced in the amorphous matrix during the PLA process, as estimated from the spatial correlation model using the line center position and the asymmetry in the LO phonon, is found to increase with the annealing power density. The threshold annealing power density for complete regrowth of crystallinity for ion-implanted GaAs is also reported in this article. It is also found that, for higher implantation fluences, the Raman spectra for P-ion-implanted, PLA GaAs show a phosphorus localized vibrational mode (PLVM) of substitutionally incorporated phosphorus, which is absent for lower implantation fluences.

II. EXPERIMENTAL PROCEDURE

Raman scattering experiments were performed in the backscattering geometry by employing the 496.5-nm wavelength of the argon-ion laser, the RAMANOR double monochromator, and the usual photon counting electronics. The ⟨100⟩ face of a 350-μm thick semi-insulating GaAs sample with a resistivity of 10^7 Ω cm was implanted with 70 keV P-ions at various implantation fluences ranging from 5×10^{12}

[a]Electronic mail: pverma@physics.iitd.ernet.in

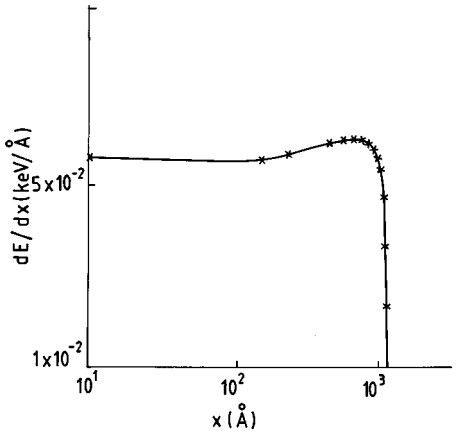

FIG. 1. Variation of the rate of energy loss of 70 keV P-ion in GaAs with distance from the surface.

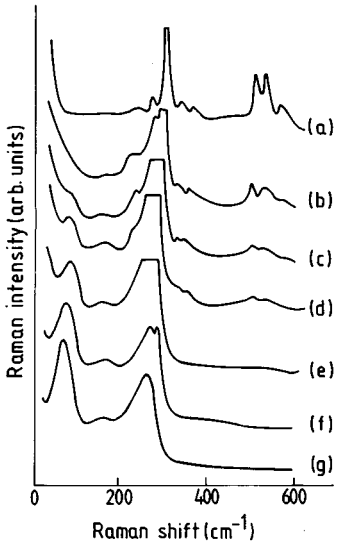

FIG. 2. Room temperature Raman spectra of P-implanted GaAs for implantation fluences (a) *c*-GaAs, (b) 5×10^{12}, (c) 1×10^{13}, (d) 7×10^{13}, (e) 5×10^{14}, (f) 1×10^{15}, and (g) 5×10^{15} ions/cm^2.

to 5×10^{15} ions/cm^2. The distribution of implanted ions can be estimated from the differential energy loss of the incident ions in the target during the implantation process. The energy loss curve for 70 keV P-ions in GaAs is shown in Fig. 1. It is estimated from Fig. 1 that maximum disorder would occur at a depth between 300 and 700 Å. The penetration depth d, of the probing laser in GaAs can be calculated in terms of the absorption coefficient α, as $d=1/2\alpha$. Using the values of absorption coefficient estimated by Aspnes *et al.*,[9] the penetration depth for $\lambda=496.5$ nm in GaAs is ~450 Å. Therefore, by using this laser wavelength for the Raman experiments, we are able to probe the maximum disordered portion of the 70-keV P-implanted GaAs sample.

The implanted samples were subsequently annealed using the 1.06-μm wavelength of a Q-switched Nd:YAG laser with pulse width of 90 ns at various power densities ranging from 8 to 20 MW/cm^2. The annealing laser at $\lambda=1.06$ μm is below the band gap of crystalline GaAs (*c*-GaAs), and hence a *c*-GaAs sample is essentially transparent to this light. A disordered material is a high energy system, and thus its band gap is low, the value of which would depend upon the degree of disorder. Our experiments show that the 70-keV P-implanted GaAs sample is opaque to the $\lambda=1.06$-μm line. Thus the band gap of this implanted sample has become <1.16 eV (1.06 μm). Therefore, when the sample is annealed with the 1.06-μm laser line, only the disordered region of the sample absorbs light and the remaining crystalline part of the sample is transparent. This means that the annealing laser is selectively absorbed in the amorphous region, and only this portion of the sample melts and undergoes the annealing process. Since the crystalline part of the sample does not melt during the annealing process, we do not expect any noticeable diffusion of P-ions deeper into the sample during the annealing process.

It was observed in a separate experiment, where change in reflectivity was measured as a function of time during the pulse laser annealing of GaAs, that the molten phase duration was approximately equal to or slightly more than (depending upon the laser power) the pulse width of annealing laser. The annealing laser pulse width in this experiment was 90 ns. Thus the molten region of the sample during the PLA process is expected to last approximately up to 100 ns.

The laser beam in the annealing process was focused to a 100-μm diameter spot which was raster scanned over the sample surface by employing a computer controlled microtranslator with 50 μm steps to produce a continuously overlapped annealed region of 2×2 mm^2. The center of this annealed region was probed by tightly focussed (100 μm) laser beam in the Raman experiment. The penetration depth of the probing Ar-ion laser beam is comparable to the implanted and the laser annealed depths, which ensures that the Raman signal is obtained only from the implanted and annealed part of the sample. The experiments were performed at room temperature in a vacuum chamber. The monochromator was calibrated using the strong plasma lines of the Ar-ion laser.

III. EXPERIMENTAL RESULTS AND DISCUSSION

A. Phosphorus ion implantation

The topological disorder produced in GaAs due to P-ion implantation ranges from point defects to complete amorphous state as the implantation fluence is varied from 5×10^{12} to 5×10^{15} ions/cm^2. The Raman spectra of unimplanted *c*-GaAs is dominated by the sharp ($q=0$) LO-phonon line at 291.5 cm^{-1} at room temperature. The effect of disorder on the first-order Raman mode of GaAs is to cause softening and asymmetric broadening of the allowed LO-phonon line. The intensity ratio, $I_{\mathrm{LO}}/I_{\mathrm{TO}}$, which can be used as a measure of crystallinity, is found to decrease with increase in implantation fluence.

Figure 2 displays room temperature Raman spectra for 70 keV P-ion-implanted GaAs for fluences ranging from 5×10^{12} to 5×10^{15} ions/cm^2. The one-phonon modes between 250 and 300 cm^{-1} in Fig. 2 are arbitrarily truncated at the top in order to focus attention on the two-phonon modes, and hence the one-phonon modes are out of scale. Focusing attention on the one-phonon structures, Fig. 3 shows the

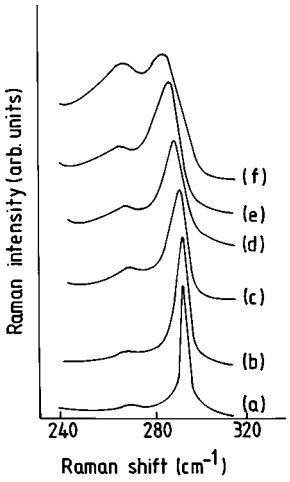

FIG. 3. One-phonon optical modes in the Raman spectra of P-implanted GaAs for implantation fluences (a) *c*-GaAs, (b) 5×10^{12}, (c) 1×10^{13}, (d) 7×10^{13}, (e) 5×10^{14}, and (f) 1×10^{15}.

changes in intensity, shift, and asymmetric broadening. The Raman spectra for *c*-GaAs are shown in Figs. 2(a) and 3(a), Figs. 2(b)–2(f), and 3(b)–3(f) show the effects of increasing disorder, and Fig. 2(g) shows the Raman spectrum of completely amorphized GaAs (*a*-GaAs). All modes become optically allowed due to a break-down in the momentum selection rules in the disordered material. The first-order acoustic modes, which are not allowed in the Raman spectrum of *c*-GaAs, are very prominent in the *a*-GaAs between 20 and 100 cm^{-1}. The evolution of the spectra of Fig. 2, with increasing implantation fluences, exhibits the disappearance of sharp phonon modes and development of a broad three-band continuum, shown in Fig. 2(g). The intensity of the allowed one-phonon mode at 291.5 cm^{-1} decreases, while its width and asymmetry increases and the mode shifts towards lower frequency side. The intensity of the forbidden TO mode at 268 cm^{-1} increases and it tends to merge into the LO mode to give a broad structure $\sim$250 cm^{-1}. The intensity ratio, $I_{\mathrm{LO}}/I_{\mathrm{TO}}$, which is about 41 for *c*-GaAs in our experiments, rapidly decreases with implantation fluence and becomes almost one for implantation fluence of 1×10^{15} ions/cm^2. The low-frequency broad band appears due to the one-phonon acoustic modes, which are symmetry-forbidden in *c*-GaAs, and the structure $\sim$250 cm^{-1} is due to the combined density-of-states of all other possible phonons. This is the Raman signature of amorphization.

The two-phonon modes show their sensitivity towards the increasing disorder by rapid decrease in their intensity till they vanish completely in Fig. 2(e) at an implantation fluence of 5×10^{14} ions/cm^2. The one-phonon mode disappears completely in the Raman spectrum at an implantation fluence of 5×10^{15} ions/cm^2 in Fig. 2(g), which can be estimated as the threshold fluence for the crystalline to amorphous transition for the sample. The threshold fluence for the disappearance of the first-order mode is greater by an order of magnitude than that for the disappearance of second-order modes. The zone edge phonons (ZEPs) are more susceptible to any disorder in the lattice structure compared to the zone center phonons (ZCPs). Thus the two-phonon modes involving ZEPs are more sensitive to ion implantation than the one-phonon LO mode which is a ZCP. This gives rise to two different threshold fluences for one-phonon and two-phonon modes.

The radiation damage induced by ion implantation leads to a topological disorder in the lattice and the periodicity of the single crystal breaks up. The propagation of phonons becomes confined to a small region, and so the phonon correlation length decreases, the value of which depends upon the degree of disorder. This leads to, apart from a broadening and softening of the LO phonon, a decrease in the intensity of the allowed LO phonon and an enhancement in the intensity of the forbidden TO phonon. In addition, the asymmetry of the LO phonon, Γ_a/Γ_b, which is the ratio of the half-widths on the low-frequency side to the high-frequency side of the maximum, is also found to increase with increasing fluence. All these changes can be explained by a simple model based on spatial correlation.[2,10] This treatment accounts for the effects of spatial inhomogeneity on the line shape of the LO phonon spectrum. The spatial correlation length is very large (ideally, infinity) for a crystalline material, which leads to the $q=0$ momentum selection rule for the first-order modes. The correlation length is confined to a finite range for a topologically disordered material, which leads to relaxation of momentum selection rules. In a disordered material, one can identify a finite correlation region over which the crystalline order exists. The disorder disrupts the long-range ionic ordering which weakens the Coulomb interaction, which is responsible for the LO–TO phonon splitting. Thus the reduction of correlation length of the LO phonon shifts its energy nearer to that of the TO phonon as the disorder increases. This qualitatively explains the softening and broadening of the LO phonon. The softening and broadening of the LO phonon with disorder continues until a threshold implantation fluence is reached when the material becomes amorphous. In fact, the isolated damage clusters and amorphous regions at low implantation fluence overlap to yield a continuous amorphous layer at threshold fluence.

In order to explain the changes in the LO-phonon line shape and position on the basis of the spatial correlation model,[2] we assume that the regions where the crystalline order exists in the disordered material, are spherical in shapes and are separated by thin region of amorphous material. The Raman signal in our experiments is averaged over a laser illumination spot of diameter nearly 100 μm, thus our experiments are not sensitive to the exact shapes of the crystallites. Assuming that the correlation length[2] is given by L, and taking the spherical symmetry into consideration, the Raman intensity $I(\omega)$, at a frequency ω, can be given[10] as

$$I(\omega)\propto\int_0^1 \exp\left(-\frac{q^2L^2}{4}\right)\frac{4\pi q^2\,dq}{[\omega-\omega(q)]^2+\left(\frac{\Gamma_0}{2}\right)^2}, \qquad (1)$$

where q is expressed in units of $2\pi/a$, a is the lattice constant, Γ_0 is the natural linewidth for the crystal and L is the diameter of the correlation region, which gives the estimated size of microcrystals. A dispersion $\omega(q)=A+B\cos(\pi q)$, with $A=269.5$ cm^{-1} and $B=22.5$ cm^{-1} reproduces the actual dispersion of the LO phonon in GaAs along the $\langle100\rangle$

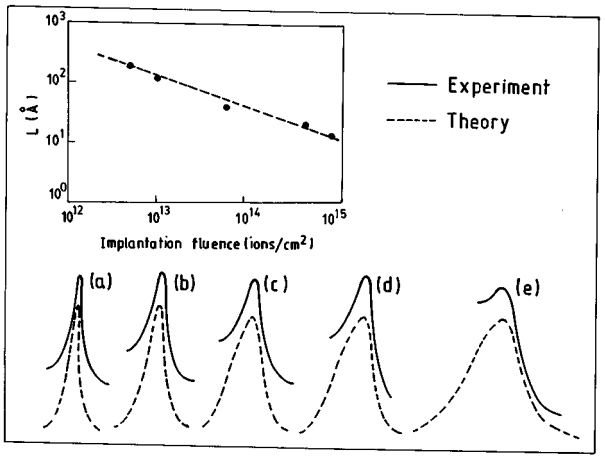

FIG. 4. Experimental and theoretical LO-phonon line shape for implantation fluence (a) 5×10^{12}, (b) 1×10^{13}, (c) 7×10^{13}, (d) 5×10^{14}, and (e) 1×10^{15} ions/cm^2. The inset shows coherence lengths at various implantation fluences. The broken line in the inset is a guide line to the eye.

direction.[2] Equation (1) gives the Raman intensity for the LO phonon as a function of frequency ω for a particular value of the correlation length L. For each implantation fluence, the value of L is properly chosen so that the theoretical line shape calculated from Eq. (1) matches well with the experimental line shape. Figure 4 shows the theoretical and experimental line shapes for various implantation fluences. The base line of the experimental line shapes are shifted in Fig. 4 to distinguish between theoretical and experimental lines. For higher implantation fluences [spectra (d) and (e) in Fig. 4], the TO phonon dominates, and so the matching between experimental and theoretical curves is not very good at the lower frequency side of the line center. The inset in Fig. 4 shows the estimated values of the correlation length at various implantation fluences.

The shift and broadening of the LO phonon as a function of implantation fluence are shown in Fig. 5(a). Figure 5 shows an increase in the phonon linewidth and a down-shift of line position with increasing implantation fluence, which

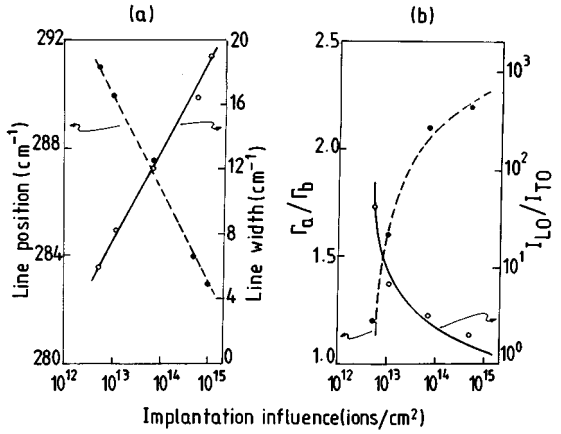

FIG. 5. Implantation fluence dependence of the line center and linewidth for LO-like phonon in P-implanted GaAs, (b) implantation fluence dependence of the asymmetry Γ_a/Γ_b and intensity ratio I_{LO}/I_{TO} for LO-like phonon in P-implanted GaAs.

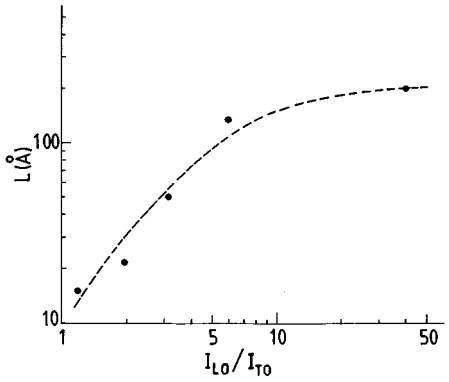

FIG. 6. The estimated values of the coherence length in ion-implanted GaAs for various observed values of the intensity ratio, I_{LO}/I_{TO}, in the Raman spectrum. The broken line is a guide line to the eye.

is due to the fact that the increasing implantation fluence decrease the size of crystalline order and the phonon correlation length. Figure 5(b) gives the asymmetry Γ_a/Γ_b and the intensity ratio I_{LO}/I_{TO} at various implantation fluences. The asymmetry as high as 2.2 and the intensity ratio close to 1 can be seen in Fig. 5(b) for an implantation fluence of 1×10^{15} ions/cm^2, which are, respectively, 1 and 41 for c-GaAs. Thus the intensity ratio, I_{LO}/I_{TO} can be used as a measure of crystallinity. Lower value of the intensity ratio indicates higher lattice disorder. For higher implantation fluence, the sample becomes complete amorphous and one-phonon modes are no longer distinguishable. Figure 6 shows the estimated value of the correlation length at various observed values of the intensity ratio I_{LO}/I_{TO}. The broken line in Fig. 6 is a guideline to the eye. This curve can be utilized to estimate the size of microcrystal generated by ion implantation for an observed value of the intensity ration, I_{LO}/I_{TO} in its Raman spectrum.

B. Pulse laser annealing

The GaAs sample implanted with 70 keV P-ions to a dose of 5×10^{15} ions/cm^2 was annealed using the 1.06-μm wavelength of a Q-switched Nd:YAG laser with power densities ranging from 8 to 20 MW/cm^2. The gradual transformation of a-GaAs into almost c-GaAs during the annealing process was monitored by Raman scattering. It is well accepted[11] that the mechanism involved in PLA is liquid phase epitaxy (LPE) where the molten layer is found to last approximately up to the pulse width of the annealing laser. For low power density of the annealing laser, a small amount of energy is transferred to the sample and this energy flows rapidly into the sample. Thus only a very small area of the sample, where the laser pulse is shot, may undergo LPE and achieve the crystalline structure. Due to the small size of molten layer for a very short time at low annealing power density, the annealed area becomes a cluster of microcrystals. The surrounding area still remains amorphous. As the annealing power density is increased, the size of molten layer increases and it remains molten for comparatively longer time. The annealed layer thus obtained has longer crystalline order. When the threshold of annealing power density is

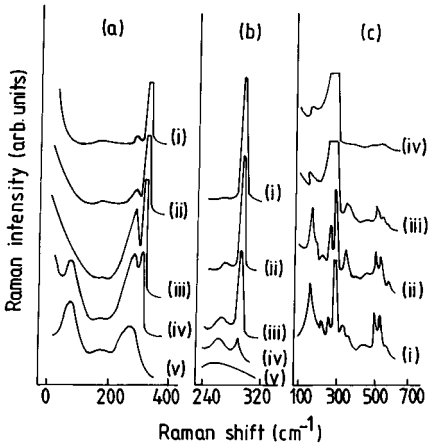

FIG. 7. Raman spectra of P-implanted GaAs at a dose of 5×10^{15} ions/cm^2 and subsequently PLA at various annealing power densities. Spectrum (i) in (a)–(c) correspond to the *c*-GaAs, spectrum (ii), (iii), and (iv) in (a)–(c) are for annealing power densities 20, 15, and 8 MW/cm^2, respectively, and spectrum (v) in (a) and (b) are for *a*-GaAs.

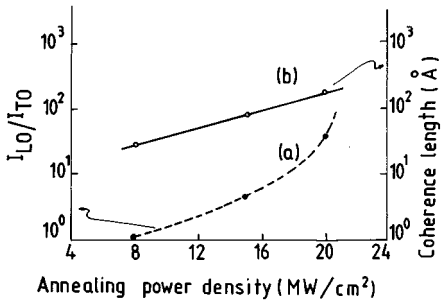

FIG. 8. The annealing power density dependence of (a) intensity ratio I_{LO}/I_{TO} and (b) coherence length in the PLA process of P-implanted GaAs.

achieved, the entire annealed area becomes crystalline. Thus the phonon coherence length, which had become very small during the implantation process, again starts increasing with increase in annealing power density.

Figure 7 illustrates the effects of PLA on the Raman spectra at various annealing power densities. The overall structures between 20 and 300 cm^{-1}, the one-phonon optic modes between 250 and 300 cm^{-1} and the weak two-phonon structures between 100 and 600 cm^{-1} are shown in Figs. 7(a)–7(c), respectively. Spectra (i) in Fig. 7 are for *c*-GaAs and spectra (ii) are for the best annealed spots for annealing power density of 20 MW/cm^2. Spectra (v) in Figs. 7(a) and 7(b) are from the unannealed portion of the sample. For annealing power densities <8 MW/cm^2, no change is seen in the Raman spectrum of the sample. As the power density is increased to 8 MW/cm^2, as shown by spectra (iv) in Figs. 7(a)–7(c), a LO-like mode at 286 cm^{-1} and a TO-like mode at 264 cm^{-1}, which is much broader, start appearing and their intensities are almost equal, making the intensity ratio, I_{LO}/I_{TO} almost one. This shows that the sample has large amount of implantation induced damage and hence the selection rules are relaxed. This is also evident from the appearance of one-phonon acoustic mode at low frequency. The large asymmetry and the down-shift in LO-phonon position by 5.5 cm^{-1} shows that the annealing process has created small crystallites, due to which the correlation length is very small. The two-phonon acoustic modes in Fig. 7(c), between 100 and 200 cm^{-1} starts building up with weak intensity. The two-phonon combination modes between 300 and 490 cm^{-1} are observed with diminished intensity. The overtones of the optic modes between 490 and 600 cm^{-1} have almost negligible intensity, but show their presence. All these clearly indicate that the recrystallization process has started.

For the annealing power density of 15 MW/cm^2, the LO mode shoots up rapidly and shifts toward the LO frequency of a *c*-GaAs. The line asymmetry and the linewidths are decreased and the intensity ratio I_{LO}/I_{TO} increases rapidly. The structure between 20 and 100 cm^{-1} almost disappears. All the two-phonon modes are further developed, but still they are weak and broader. An additional structure, corresponding to the PVLM, starts appearing near 347 cm^{-1}. The remaining asymmetry, shift and diminished intensity of different phonon modes indicate that the annealed crystallites are still small in size and the annealed region is partly amorphous.

The sample almost recovers its crystalline structure, as shown by spectra (ii) in Figs. 7(a)–7(c) for annealing power density of 20 MW/cm^2. The forbidden TO mode appears with very weak intensity, the LO mode becomes more intense and appears at 291 cm^{-1}, and the two modes become narrower and symmetric. The intensity ratio, I_{LO}/I_{TO} is increased to $\sim$39. The two-phonon structures are fully grown and are almost same as those for *c*-GaAs. A careful examination of the spectra (i) and (ii) in Figs. 7(a)–7(c) indicates that the two are not exactly the same. Further increase in annealing power density does not have any appreciable change on the phonon structures. The slight difference in the phonon structures in the two spectra is predominantly due to two reasons, first, due to the presence of phosphorus impurity at substitutional lattice site, and second, due to the possibility of inhomogeneous annealing, as the annealing pulse has a spot size of 100 μm and is advanced by 50 μm in each step. The oscillator strength of the PLVM increases and it becomes narrower, symmetric and shifts to 350 cm^{-1}. The quality of the annealed layer can be investigated by the PLVM, since an incomplete annealing will cause an increase in the width of the PLVM (Ref. 12) and these are seen as a deviation from tetrahedral bounding symmetry of the implanted impurity. The appearance of narrow and symmetric PLVM is a clear indication of complete annealing. There are no changes in the PLVM on further increasing the power density. Therefore, we believe that 20 MW/cm^2 is the threshold value of annealing power density for the recrystallization of the sample.

The intensity ratio, I_{LO}/I_{TO} gives a quantitative measure of the lattice regrowth. Figure 8(a) gives the intensity ratio, I_{LO}/I_{TO} with respect to the annealing power density, which changes from 1 to 39 as the annealing power density is increased. It can be seen from Fig. 8(a) that the sample achieves crystallinity faster when the annealing power density approaches the threshold value. The size of the phonon correlation length (which is also the microcrystallite size) is calculated for various annealing power densities using Eq.

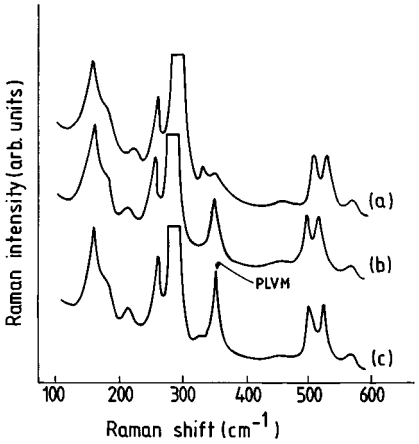

FIG. 9. Raman spectra of P-implanted and PLA GaAs showing the PLVM for implantation fluence (a) 1×10^{15}, (b) 5×10^{15}, and (c) 1×10^{16} ions/cm^2.

(1). Figure 8(b) displays the estimated microcrystallite size with respect to the annealing power density in the PLA process. The microcrystallite size is estimated to be 30 Å for annealing power density of 8 MW/cm^2 and increased to ~250 Å for the annealing power density of 20 MW/cm^2. A curve, similar to one in Fig. 6, between the observed value of I_{LO}/I_{TO} and the corresponding value of the coherence length for the annealing process can be estimated, which can be used to estimate the size of microcrystal for experimentally observed value of the intensity ratio, I_{LO}/I_{TO} in the Raman spectrum of the sample.

Light impurities in GaAs are known[12–14] to give rise to localized vibrational modes (LVM). The substitution of impurities into lattice site after PLA gives rise to such LVM. The vibrational energy of LVM for these light impurities is extremely localized, generally extending over less than one lattice constant, and hence, these modes provide a sensitive measure of short range lattice order. It plays an important role in the investigation of the annealed layer, since incomplete annealing will cause an asymmetric increase in the width of the LVM. It can be identified from the Raman spectrum, whether the impurities occupy the substitutional lattice sites or the interstitial sites, since the frequency of the PLVM arising from the two sites will be different. Phosphorus substituting for As in GaAs has tetrahedral nearest-neighbor symmetry and produces a fundamental band around 354 cm^{-1}.[15] The PLVM is observed approximately at this position and so we believe that the phosphorous impurities at the interstitial sites are negligible. The PLVM is observed only above a certain value of implantation fluence in this study, and it could not be observed up to an implantation fluence of 1×10^{15} ions/cm^2. The intensity of the PLVM for fluence up to 1×10^{15} ions/cm^2 must be very weak and thus is buried in the combination modes of *c*-GaAs at 336 and 366 cm^{-1}. The Raman spectra of the best annealed spot of a GaAs sample implanted with 70 keV P-ions at various implantation fluences are shown in Fig. 9. The Raman spectra show the presence of symmetric PLVM and complete recovery of two-phonon structures confirming proper annealing of the samples. The combination modes between 300 and 400 cm^{-1} in Fig. 9(a) for implantation dose of 1×10^{15} ions/cm^2 are weak due to the PLVM falling in the same frequency range, but due to very weak intensity, the PLVM is not observed. The presence of PLVM with a small peak at 350 cm^{-1} is seen for the implantation fluence of 5×10^{15} ions/cm^2 in Fig. 9(b). The combination modes are modified and buried in the comparatively strong PLVM. As the fluence is increased to 1×10^{16} ions/cm^2 in Fig. 9(c), due to the presence of more phosphorus ions, the PLVM becomes more intense and appears at 352 cm^{-1}. The combination modes are completely hidden. The difference of 2 cm^{-1} between the calculated[15] and observed values of PLVM frequency is probably due to some point defects present in the annealed layer.

IV. CONCLUSIONS

The ZEPs are more sensitive to the topological disorder than the ZCPs. The threshold value of implantation fluence for the one-phonon mode is estimated to be greater than that for the two-phonon modes by an order of magnitude. The one-phonon modes shift downwards, broaden asymmetrically, the intensity ratio I_{LO}/I_{TO} decreases from 41 to ~1, and the phonon correlation length for the LO phonon decreases as the spatial disorder increases. A curve between the correlation length and the intensity ratio, I_{LO}/I_{TO}, gives a quantitative measure for the degree of disorder. Incomplete annealing in the PLA process creates microcrystals, size of which depends upon the annealing power density. The intensity ratio I_{LO}/I_{TO} is close to 1 when the lattice reconstruction process starts and increases to 39 when the annealing power density reaches its threshold. The threshold value of annealing power density is estimated to be 20 MW/cm^2 for 70 keV phosphorus implantation at a fluence of 5×10^{15} ions/cm^2. The PLVM could not be clearly observed in the PLA samples for implantation fluences up to 1×10^{15} ions/cm^2 due to insufficient amount of impurity. For increased impurity ions at higher fluences, the PLVM for substitutionally incorporated P-ions is observed, and is found to give a very sensitive measure for lattice reconstruction.

[1] T. Nakamura and T. Kotada, J. Appl. Phys. **53**, 5870 (1982).
[2] K. K. Tiong, P. M. Amrithraj, F. H. Pollak, and D. E. Aspnes, Appl. Phys. Lett. **44**, 122 (1984).
[3] C. W. White, S. R. Wilson, B. R. Appleten, and F. W. Young, Jr., J. Appl. Phys. **51**, 738 (1980).
[4] J. Krynicki, J. Suski, S. Ugniewoki, R. Grotzschol, R. Klabes, U. U. Kreissing, and J. Rudiger, Phys. Lett. A **61**, 181 (1977).
[5] K. P. Jain, A. K. Shukla, R. Ashokan, S. C. Abbi, and M. Balkanski, Phys. Rev. B **32**, 6688 (1985).
[6] G. Carter and W. A. Grant, *Ion Implantation of Semiconductors* (Pitman, New York, 1976), pp. 189–194.
[7] D. R. Myers, P. L. Gourley, and P. S. Peercy, J. Appl. Phys. **54**, 5032 (1983).
[8] E. I. Shtyrokoa, I. B. Khaolbullin, M. M. Zaripov, M. F. Galyoutdinoy, and R. M. Bayazitov, Sov. Phys. Semicond. **9**, 1309 (1976).
[9] D. E. Aspnes and A. A. Studna, Phys. Rev. B **27**, 985 (1983).
[10] R. Ashokan, K. P. Jain, H. S. Mavi, and M. Balkanski, J. Appl. Phys. **60**, 1985 (1986).
[11] D. H. Loundes, *Semiconductors and Semimetals* (Academic, New York, 1984), Vol. 23, p. 471.
[12] L. H. Skolink, W. G. Spitzer, A. Kahan, and R. G. Hunsperger, J. Appl. Phys. **42**, 5223 (1971).
[13] W. M. Theis and W. G. Spitzer, J. Appl. Phys. **54**, 890 (1984).
[14] T. Nakamura and T. Katoda, J. Appl. Phys. **57**, 1084 (1985).
[15] K. P. Jain and A. K. Prabhakaran, Phys. Rev. B **8**, 1503 (1973).